

December 22, 1994

**CHARGED PARTICLE PSEUDORAPIDITY DISTRIBUTIONS  
IN Au+Al, Cu, Au, and U COLLISIONS AT 10.8 A·GeV/c**

E877 Collaboration

J. Barrette<sup>4</sup>, R. Bellwied<sup>8</sup>, S. Bennett<sup>8</sup>, P. Braun-Munzinger<sup>6</sup>,  
W. E. Cleland<sup>5</sup>, M. Clemen<sup>5</sup>, J. D. Cole<sup>3</sup>, T. M. Cormier<sup>8</sup>, G. David<sup>1</sup>,  
J. Dee<sup>6</sup>, O. Dietzsch<sup>7</sup>, M. W. Drigert<sup>3</sup>, J. R. Hall<sup>8</sup>, T. K. Hemmick<sup>6</sup>,  
N. Herrmann<sup>2</sup>, B. Hong<sup>6</sup>, Y. Kwon<sup>6</sup>, R. Lacasse<sup>4</sup>, A. Lukaszew<sup>8</sup>, Q. Li<sup>8</sup>,  
T. W. Ludlam<sup>1</sup>, S. K. Mark<sup>4</sup>, S. McCorkle<sup>1</sup>, R. Matheus<sup>8</sup>,  
J. T. Murgatroyd<sup>8</sup>, E. O'Brien<sup>1</sup>, S. Panitkin<sup>6</sup>, T. Piazza<sup>6</sup>, C. Pruneau<sup>8</sup>,  
M. N. Rao<sup>6</sup>, M. Rosati<sup>4</sup>, N. C. daSilva<sup>7</sup>, S. Sedykh<sup>6</sup>, U. Sonnadara<sup>5</sup>,  
J. Stachel<sup>6</sup>, N. Starinsky<sup>4</sup>, E. M. Takagui<sup>7</sup>, S. Voloshin<sup>5,a</sup>, G. Wang<sup>4</sup>,  
J. P. Wessels<sup>6</sup>, C. L. Woody<sup>1</sup>, N. Xu<sup>6</sup>, Y. Zhang<sup>6</sup>, C. Zou<sup>6</sup>

1. Brookhaven National Laboratory, Upton, NY 11973
2. Gesellschaft für Schwerionenforschung, Darmstadt, Germany
3. Idaho National Engineering Laboratory, Idaho Falls, ID 83415
4. McGill University, Montreal, Canada
5. University of Pittsburgh, Pittsburgh, PA 15260
6. State University of New York, Stony Brook, NY 11794
7. Universidade de São Paulo, São Paulo, Brazil
8. Wayne State University, Detroit, MI 48202

---

<sup>a</sup>On leave from Moscow Engineering Physics Institute, Moscow, 115409, Russia

## ABSTRACT

We present the results of an analysis of charged particle pseudorapidity distributions in the central region in collisions of a Au projectile with Al, Cu, Au, and U targets at an incident energy of 10.8 GeV/c per nucleon. The pseudorapidity distributions are presented as a function of transverse energy produced in the target or central pseudorapidity regions. The correlation between charged multiplicity and transverse energy measured in the central region, as well as the target and projectile regions is also presented. We give results for transverse energy per charged particle as a function of pseudorapidity and centrality.

PACS number(s): 13.85.-t, 25.75.+r

## 1 Introduction

Global observables such as (pseudo-)rapidity particle density contain valuable information on the reaction dynamics and, indirectly, on the degree of thermalization as well as the energy and entropy densities reached in relativistic nucleus-nucleus collisions. With light projectiles, pseudorapidity distributions have been studied in detail previously both at AGS and CERN energies (for a review, see Ref. [1]). Our collaboration earlier reported the measurements of charged particle distributions [2], energy flow and stopping [3], transverse energy distributions [4], in the collisions of a Si beam with Al, Cu, and Pb targets. Large energy deposition has been inferred from these measurements. Extrapolating these results to heavy projectiles raises expectations to create, in these collisions, the deconfined phase of quarks

and gluons. We report here measurements of the charged particle pseudorapidity distributions in collisions of  $10.8\text{-}A$  GeV/c Au beams with several nuclear targets carried out in Experiment 877 operating at the Brookhaven National Laboratory Alternating Gradient Synchrotron (AGS). We combine the multiplicity data with our earlier measurements [4] of transverse energy ( $E_t$ ) pseudorapidity distributions in Au+Au collisions at the same energy to study the  $E_t$  per charged particle as a function of pseudorapidity and the centrality of the collision.

## 2 Experimental setup

The E877 experimental setup is shown schematically in Fig. 1. For the pseudorapidity distribution analysis we use data primarily from the Multiplicity Detector, complemented by data from the Participant and Target Calorimeters (see the insert in Fig. 1), which provide a measurement of the centrality of a collision. “Zero-degree” energy (deposited mainly by projectile spectators) is measured by the Uranium Calorimeter, situated in the forward spectrometer. The horizontal position of the beam particle is measured by a pair of silicon strip detectors, the Beam Vertex Detectors, shown in the insert in Fig. 1 (BVer 1 and BVer 2). The information from these detectors is used on an event by event basis. The mean vertical displacement of the incoming beam particle is estimated using the information on the distribution of the “centroid of hits” in the multiplicity counter (see details in Section 3). The angular divergence of the beam ( $\sim 1$  mr) is much smaller than the bin widths in  $\eta$  and  $\phi$  used for multiplicity distribution analysis. Most of

upstream interactions are effectively rejected using the pulse height from a 100  $\mu\text{m}$  thick Si surface barrier detector located just upstream of the target.

The Multiplicity Detector, shown in Fig. 2, consists of two identical silicon pad detectors, each of which was made from a disc of silicon 300  $\mu\text{m}$  thick and approximately 3.8 cm in radius. To reduce the number of  $\delta$ -electrons reaching these detectors, two 3 mm thick aluminum absorber plates were placed upstream of each plane of silicon. The active region of each detector is a ring of inner radius 1.4 cm and outer radius 3.4 cm divided into 512 pads. The detectors are segmented into 8 concentric rings of 64 pads each. One detector, located 3.37 cm from the target, covers the pseudorapidity region  $0.87 < \eta < 1.61$ , and the other, located 8.17 cm from the target, covers the region  $1.61 < \eta < 2.46$ . These values of pseudorapidity coverage correspond to the case where the beam particle is incident at the center of the detector. Due to the finite size of the beam spot and variation of the beam position during the AGS spill, the actual pseudorapidity coverage is slightly larger. The size of the pads corresponds approximately to 0.1 in both  $\eta$  and azimuthal angle  $\phi$ , which determines the angular resolution in this measurement. Signals from the pads, after preamplification and shaping, are sampled at the peak and digitized. For the most central events the mean occupancy in pads which see the highest track density is close to 0.3.

The Participant Calorimeter (PCal) [5] is a lead/iron/scintillator sampling calorimeter. It has a depth of four interaction lengths and a radius of approximately 84 cm. It is approximately azimuthally symmetric, built with four identical quadrants. Each quadrant of the PCal is divided into four azimuthal slices of  $22.5^\circ$ . Each slice is divided radially into eight towers.

Longitudinally, the calorimeter is divided into two electromagnetic depth segments and two hadronic depth segments. This division leads to a total of  $16 \times 8 = 128$  towers for each quadrant and 512 towers for the entire calorimeter. PCal measures energy flow into the polar angle region which corresponds to pseudorapidity range  $0.83 < \eta < 4.7$ . The Target Calorimeter (TCal) is made of 992 NaI crystals each 5.3 radiation length deep. It covers the backward hemisphere, corresponding to the pseudorapidity range  $-0.5 < \eta < 0.8$ . For more details on TCal and the analysis of TCal data see [3,6]. The Uranium Calorimeter (UCal) consists of 25 modules and measures the energy of particles entering the forward spectrometer through a collimator with an opening of  $-115 \text{ mr} < \theta_x < 14 \text{ mr}$  and  $-21 \text{ mr} < \theta_y < 21 \text{ mr}$ .

The data were taken with several targets, Al (242 mg/cm<sup>2</sup>, approximately 1.9% of an interaction length for a gold projectile), Cu (500 mg/cm<sup>2</sup>,  $\approx 2\%$ ), Au (540 mg/cm<sup>2</sup> and 980 mg/cm<sup>2</sup>,  $\approx 1\%$  and 1.8%), and U (575 mg/cm<sup>2</sup> and 1150 mg/cm<sup>2</sup>,  $\approx 1\%$  and 2%).

## 3 Analysis

### 3.1 Pulse height spectra

The pulse height distributions in the Multiplicity Detector were first corrected for pedestal offsets and differences in gain, and the non-functional channels were identified. A channel was defined as good if the pulse height distribution showed a minimum ionizing particle (m.i.p.) peak well separated from the pedestal (as in the example shown in Fig. 3). Dead or noisy chan-

nels (altogether about 25%) were removed in the analysis. The corrected pulse height distributions were studied in a variety of ways. In the vicinity of pedestals the distributions were fitted by a Gaussian; this fit gives the width of the electronic noise distribution in each particular channel, and permits to evaluate the mean occupancy of the pad ( $1 - p_0$ , where  $p_0$  is the probability of the pad not being occupied). The part of the distributions above the pedestals were fitted by a Landau distribution convoluted with a Gaussian describing the electronic noise and taking into account the effects of atomic binding of the electrons [8] (this fit is similar to the analysis done in [9]):

$$f(\Delta) = \frac{1}{\sigma\sqrt{2\pi}} \int_0^\infty f_L(\epsilon) \exp\left(-\frac{(\Delta - \epsilon)^2}{2\sigma^2}\right) d\epsilon \quad (1)$$

$$\sigma = (\delta_2 + \sigma_{noise}^2)^{1/2}; \quad (2)$$

Here  $\Delta$  is the actual energy loss, the variance  $\delta_2$  is related to the effect of electron atomic binding, and  $\sigma_{noise}^2$  is the variance of electronic noise;  $f_L(\epsilon)$  is the Landau distribution function:

$$f_L(\epsilon) = \frac{1}{\xi} \Phi(\lambda); \quad \Phi(\lambda) = \frac{1}{2\pi i} \int_{c-i\infty}^{c+i\infty} \exp(u + \ln u + \lambda u) du \quad (3)$$

$$\lambda = \frac{1}{\xi}(\epsilon - (\epsilon_{mp} - \xi\lambda_0)) = \frac{\epsilon - \epsilon_{mp}}{\xi} + \lambda_0; \quad \lambda_0 = -0.225, \quad (4)$$

where  $\xi$  is the width of the distribution, and  $\epsilon_{mp}$  is the most probable energy loss;  $c$  is an arbitrary real positive constant. For the case of multiple ( $n$ ) hits the parameters  $\xi$  and  $\epsilon_{mp}$  are to be replaced by:

$$\xi_n = n\xi \quad (5)$$

$$\epsilon_{n,mp} = n(\epsilon_{mp} + \xi \ln(n)) \quad (6)$$

To investigate the distribution in number of hits for the purpose of evaluation of mean pad multiplicity, two different fits to the pulse height distributions were carried out. The first fit assumed a Poisson distribution in the number of hits in the pad, and the parameter extracted was the mean occupancy, which can be compared with the value extracted from the fit to the electronic noise distribution. The quality of the fit can be seen in Fig. 3, where the fitted curves are shown along with the data from one of the pads.

In the second fit, the probabilities of single or double hits are free parameters. We find that the probability of double hits defined independently exceeded the value expected from Poisson statistics. For pads with mean occupancy  $\approx 0.3$  the ratio of observed double hits to the calculated value from Poisson statistics is  $\approx 1.3$ . This effect is understood to be the effect of  $\gamma$ -conversions in the target and in the absorber. The Monte Carlo simulation (described below) shows that for a heavy target (Au or U) about 5% of all hits are due to  $\gamma$ 's from  $\pi^0$  decays converting into  $e^+e^-$ -pairs. Due to the small opening angle about 30% of produced  $e^+e^-$ -pairs occupy the same pad of the multiplicity detector, introducing a non-Poissonian element in the distribution. The correction for  $\gamma$ -conversions used in the analysis which takes this effect into account is described below.

After the calibration was done and the procedure for the calculation of the mean pad multiplicity was established, a ‘‘hit’’ threshold was introduced corresponding approximately to one-half of the peak of the minimum ionizing particle signal. By varying the threshold position and comparing the results with the information from the fit to the electronic noise distribution, it was found that the occupancy can be defined in this way with an accuracy better

than 2%.

## 3.2 Corrections and Selection Criteria

*Event selection.* In order for an event to contribute to the multiplicity analysis, it is necessary to obtain the horizontal position of the beam particle. Thus events with missing or ambiguous information from the vertex detector were rejected. Also, it is important to reduce the background from interactions upstream of the target as much as possible. Therefore, we reject events in which the pulse height in the upstream silicon detector is below a threshold value close to the energy loss peak of Au ions.

*Beam position.* To calculate the pseudorapidity corresponding to each pad the knowledge of the position of the interaction point relative to the multiplicity detector is very important. As mentioned above, the horizontal position is measured for each event in the Beam Vertex Detector. The following technique was used to define the relative position of the Beam Vertex Detector with respect to the Multiplicity Detector. We exploit the fact that the hit centroid distribution is expected to be axially symmetric when the beam particle is incident at the center of the Multiplicity Detector. In each event the horizontal and vertical components of the hit centroid position are given by

$$C_H = \sum_i \cos \phi_i; \quad C_V = \sum_i \sin \phi_i, \quad (7)$$

where the sum is over all hits and  $\phi_i$  is the azimuthal angle of the pad containing the  $i$ -th hit. To avoid a bias in this part of the analysis from dead pads, a symmetrized dead pad mask was used, declaring some good pads as



dead to make the distribution of dead pads symmetric. After the coordinates of the centroid are calculated, the horizontal component is plotted against the position provided by the Beam Vertex Detector. The results of this analysis are shown in Fig. 4. The beam position from BVer corresponding to  $C_H = 0$  gives the the relative BVer and multiplicity detector displacement (about 0.75 mm from Fig. 4). To understand the statistical fluctuations in the plot near  $x = 0$ , note that the most probable beam position from the BVer is about  $-4$  mm; thus the beam position near zero is very rare.

The average value of  $C_V$  gives information on the mean vertical position of the beam for any event sample. A plot of  $C_H$  versus the horizontal coordinate obtained from BVer fixes the scale factor between the hit centroid position and the beam displacement. For the data shown in Fig. 4 this scale factor is 4.1 mm, which gives us about 1.2 mm for the mean vertical beam offset. One can also see from the plot that there is no correlation between vertical and horizontal components of the beam position.

The correction for multiple hits was done pad by pad using the average occupancy. Since the mean pad occupancy depends on beam position, the correction was done separately for each value of this variable. For this purpose the corresponding pseudorapidity, azimuthal angle, and solid angle in these variables were calculated for every pad as a function of both vertical and horizontal beam position. The Multiplicity Detector consists of two silicon pad detectors located at different distances from the target and covering different pseudorapidity regions. For non-zero beam positions these regions overlap. It was verified that the distributions calculated using the data from different detectors coincide in the overlapping region for the values of the

beam mean vertical displacement and the Multiplicity Detector relative offset used in the analysis. The other independent check is that the resulting azimuthal angular distributions are flat in different pseudorapidity windows. These methods are sensitive to displacements at the level of 0.2–0.3 mm.

*Upstream interactions.* Although most of the upstream interaction events are effectively rejected using the information from the upstream Si detector and the Beam Vertex Detectors, it is important for collisions of medium centrality and for data taken with light targets to perform a background subtraction to correct for residual upstream interactions. The subtraction was done using the data taken with empty target frame. The relative contamination by upstream interactions is different for events triggered by TCal or PCal. Almost all upstream interactions result in relatively low TCal  $E_t$ , but PCal  $E_t$  can be rather significant. For heavy targets the admixture of upstream interactions in the event sample is negligible for events with TCal  $E_t > 10$  GeV, and only about 20% for the region  $E_t \approx 4\text{--}5$  GeV (the corresponding differential cross section  $d\sigma/dE_t$  is presented in the following section in Fig. 8). For the Al target the admixture is about 40% in the same region (TCal  $E_t \approx 4\text{--}5$  GeV). In contrast to the heavy targets the admixture of upstream interactions for the Al target increases with TCal  $E_t$  because of the sharp drop of  $d\sigma/dE_t$  for interactions in the target; for events with TCal  $E_t > 7$  GeV, upstream interactions become dominant. For the Au target the admixture of upstream interactions in PCal  $E_t$  regions centered at 65 GeV, 130 GeV, and 190 GeV is about 70%, 40%, and 10% respectively.

*Delta electrons.* One of the most important corrections is the subtraction of hits due to  $\delta$ -electrons produced in the target. The aluminum absorber

located in front of each detector plane reduces the number of  $\delta$ -electrons by about a factor of 10, but nevertheless their contribution is not negligible. It is not possible to extract the pseudorapidity distributions of  $\delta$ -electrons (needed for the correction) directly from the data. The data for “beam” events (no interaction in the target) provide the number of produced  $\delta$ -electrons and their pseudorapidity distribution for the case when the incoming nucleus traverses the entire length of the target. Unfortunately, this distribution cannot be used for the correction for normal events, because the path length of the incoming nucleus in the target is different from that of a beam track, and thus the multiple scattering and absorption effects are also different. To understand the effect of the absorbers on the  $\delta$ -ray energy and angular distribution and to calculate the pseudorapidity distribution needed for the correction a detailed simulation was performed using the GEANT (version 3.16) package.

The GEANT results were checked by comparison with the data in several ways. The total number of produced  $\delta$ -electrons in “beam” (no interaction in the target) events and their pseudorapidity distribution were compared directly with the data for different targets and target thicknesses, and good agreement was found. For data with interactions in the target we compare the total number of  $\delta$ -electrons seen by the Multiplicity Detector. We obtain this value from the data by extrapolation of the number of hits in the Multiplicity Detector  $N_{ch}^{raw}(E_t)$  as a function of  $E_t$  to the point  $E_t = 0$  (Fig. 5) from the region  $E_t > 4$  GeV, where  $N_{ch}^{raw}$  grows linearly with  $E_t$  and the number of produced  $\delta$ -electrons does not depend on  $E_t$ . The extrapolation gives for the number of  $\delta$ -electrons values of about 13 and 24 for the 1% and 2% Au targets

respectively, which agree well with the GEANT simulation. The number of produced  $\delta$ -electrons does not depend on  $E_t$  in the region  $E_t > 4$  GeV because  $\delta$ -electrons are mostly produced by the projectile nuclei before the collision due to the relatively large value of projectile charge  $Z$ , whereas the production of  $\delta$ -electrons by final state particles is negligible. For very low  $E_t$  events one expects an increase of  $\delta$ -electron contribution to  $N_{ch}^{raw}$  due to projectile fragmentation into high  $Z$  fragments, as can be seen in Fig. 5. The value of  $N_{ch}^{raw}$  at  $E_t = 0$  corresponds to the number of  $\delta$ -electrons produced by the projectile traversing the entire target.

The GEANT  $\delta$ -electron simulations have no free parameters which affect the results. The cutoff parameters in GEANT affect the low energy part of the  $\delta$ -electron energy spectrum, but because of the absorption of low energy electrons in the aluminum absorber plates, we are insensitive to the choice of these parameters. The pseudorapidity distributions of  $\delta$ -electrons used for the corrections for 1% Au target data are shown in Fig. 6 (curves 2 and 3). At the level of accuracy required for this analysis, the distribution of  $\delta$ -electrons does not depend on the centrality of the collision.

*Gamma conversions.* Another important correction is due to  $\gamma$ -conversions in the target and absorber. This correction was calculated using FRITIOF [11] and RQMD [12] generated events combined with a GEANT simulation of the detector. In particular the ratio of pseudorapidity distributions of hits in the multiplicity detector due to  $\gamma$ -conversions and the pseudorapidity distribution of charged particles was calculated for different centralities and target thicknesses. The results do not depend on the particular event generator used. They show that for a 1% Au target approximately 5% of the charged

multiplicity seen in the multiplicity detector is due to  $\gamma$ -conversions in the target and an additional 1% is due to conversions in the absorber. The effect depends slightly on the pseudorapidity: it is about 8% in the low part of the pseudorapidity region and about 4% for high pseudorapidities. About 30% of all  $e^+e^-$ -pairs occupy the same pad of the Multiplicity Detector. This effect results in the distortion of the Poisson statistics for the hit multiplicity distribution. The distortion caused by the two-particle correlations for produced secondaries is negligible, due to the very small magnitude of the correlations [7]. The method used to correct for the  $\gamma$ -conversions is to apply the Poisson correction to the value calculated from the mean pad occupancy and then to subtract the distribution of electrons and positrons considering the pairs occupying the same pad as one charged particle. For the details of this procedure see Appendix A. The distribution used for the correction of the 1% Au target data is presented in Fig. 6 (curve 1) and has been used to obtain the charged particle multiplicity distribution for the highest centrality bin (see Fig. 9). The correction for other values of centrality scales approximately as  $dN_{ch}/d\eta$ .

## 4 Results

### 4.1 Correlations among global variables

The charged particle multiplicity measured in the Multiplicity Detector is strongly correlated with transverse energy deposited in TCal and/or PCal, and anti-correlated to the (“zero-degree”) energy deposited in UCal. We

present these correlations in Fig. 7, where we plot the uncorrected (raw) number of hits in the Multiplicity Detector versus energy in each of the detectors. The relative abundance of the events with high multiplicity is an effect of trigger thresholds. The shapes of the the distributions in TCal/PCal  $E_t$  for the events with fixed multiplicity, and the distributions in multiplicity for the events with fixed TCal/PCal  $E_t$ , are close to Gaussian distributions. The length of the crosses in Fig. 7 indicate the widths of each distribution in different regions of the plot.

The transverse energy deposited in the target (and/or central) region is strongly anticorrelated with the impact parameter of the collision. Therefore one can infer from Fig. 7 that there are no drastic changes in the charged multiplicity fluctuations between central and non-central events. The width of the correlation between charged particle multiplicity and the PCal  $E_t$ , which corresponds to the transverse energy deposited by all (charged and neutral) particles in the same pseudorapidity region, indicates that there are no large scale fluctuations in the ratio of charged and neutral particle multiplicities.

For the current analysis the TCal  $E_t$  data were used primarily as the measure of centrality of the collisions. Note that these data are almost free from contamination by upstream interactions (except for low centrality events, where the correction for upstream interactions is small but not negligible). To compare our present multiplicity data with the published  $dE_t/d\eta$  measurements in Au+Au collisions [4], we use as the measure of centrality PCal  $E_t$  data, which were effectively corrected for the leakage in the calorimeter through normalization to our previous measurements [4].

The differential cross sections in TCal  $E_t$  for different targets are shown in Fig. 8. The centrality of the collisions can be inferred using the ratio  $\sigma_{top}(E_t)/\sigma_{geom}$  (shown on bottom plate of Fig. 8), where  $\sigma_{top}(E_t)$  is defined as

$$\sigma_{top}(E_t) = \int_{E_t}^{\infty} d\sigma/dE_t dE_t, \quad (8)$$

and the geometrical cross section for the collision of  $A$  and  $B$  nuclei is  $\sigma_{geom} = \pi(R_A + R_B)^2$ ;  $R_{A,B} = 1.2A^{1/3}$  fm. The U, Cu, and Al targets data were obtained by (multilevel) triggering on PCal  $E_t$ . The width of the correlation between PCal  $E_t$  and TCal  $E_t$  is relatively large in comparison with the difference between different trigger thresholds. A special weighting technique was used to measure  $d\sigma/dE_t$ (TCal) from data triggered with PCal  $E_t$  at several thresholds (see Appendix B).

The differential cross sections  $d\sigma/dE_t$  (TCal, PCal) for the Au target agree well with our previous measurements [4]. Central collisions of Au nuclei with a U target produce about 20% more transverse energy in the TCal region than collisions with a Au target. However in the more central (PCal) region the produced transverse energy differs only by about 5%. We observe a similar difference between the two targets in the peak values of charged particle densities (see below).

## 4.2 Charged particle pseudorapidity distributions

Charged particle pseudorapidity distributions for different targets are presented in Fig. 9 for different centralities. The centrality for the different TCal  $E_t$  regions can be estimated from the ratio  $\sigma_{top}(E_t)/\sigma_{geom}$  shown in

Fig. 8. For the discussion below it is important to note that for values of  $E_t$  close to its maximum value the mean multiplicity depends weakly on the  $E_t$  cut (for Au+Au collisions this is clearly evident in Figures 5 and 7 for TCal  $E_t$  greater than 21 GeV). This suggests a simple criterion for defining the similar centralities for collisions between different projectile and target nuclei. The highest  $E_t$  bins shown in Figures 9(a)–(c) are chosen to satisfy the requirements of a weak dependence of the multiplicity on the  $E_t$  cut. These cuts correspond to values of  $\sigma_{top}(E_t)/\sigma_{geom}$  from approximately 2% for Au+Al to 0.2% for Au+U, which correspond closely to cuts used to define central events in our studies of transverse energy production [4].

We have studied the effects of systematic errors in the charged particle pseudorapidity distributions as a function of pseudorapidity. From uncertainties in the corrections to the data (beam position,  $\delta$ -rays,  $\gamma$ -conversions) we estimate the systematic error in the magnitude to be about 3% in the mid-pseudorapidity region for central Au+Au collisions. The uncertainty is slightly larger in the low pseudorapidity region (about 5%) and for lower centralities. We have also considered possible errors in the position of the peak found from Gaussian fits to the pseudorapidity distributions. These errors were evaluated by a variation of parameters in the distributions used for the corrections. It was found that the centroid of Gaussian fit is surprisingly stable for such variations. The systematic uncertainty was estimated to be not more than 0.03 units of pseudorapidity; it is mainly due to the uncertainty in the vertical position of the beam (which gives a contribution of about 0.02 units of pseudorapidity) and to the uncertainty in the correction for  $\gamma$ -conversions (also about 0.02 units). The uncertainties due to statistical



errors, are much smaller, than the systematic uncertainties.

For central and mid-central collisions and heavy targets (Au and U) the pseudorapidity distributions are well fitted by Gaussians. We show the fits for the highest  $E_t$  regions in Fig. 9 (a) and Fig. 9 (b). If we compare the fits for both targets, we see that for the U target the height is about 6% larger (about 285 and 268, respectively). The position of the peak is shifted to a lower value of pseudorapidity (1.71 for U, and 1.76 for the Au target), consistent with naive expectations for the heavier target. The distribution has the same width (about 1.05) as for the Au target. Note that the widths of analogous distributions for very central collisions of a Si beam with Al, Cu, and Pb targets [2] have very nearly the same value. For gold collisions with Cu and Al targets (Fig. 9 (c)) the shape of the distributions becomes non-Gaussian. The peaks of the distributions are shifted to the higher values of pseudorapidity, as expected for collisions with light targets.

For low centrality  $E_t$  regions the pseudorapidity distributions for Au+Au and Au+U collisions exhibit an enhancement for low pseudorapidities. Monte Carlo studies imply that this asymmetry is caused by slow protons from target fragmentation. This hypothesis was checked by studying separately pseudorapidity distributions of hits with pulse heights around the minimum ionizing peak (where one does not expect contributions from slow protons). The distributions of low pulse height hits do not show such an asymmetry; thus the low pseudorapidity enhancement appears to be entirely due to hits with high pulse heights.

We compare our results with the RQMD [12] and FRITIOF [11] event generator predictions in Fig. 10 for the most central Au+Au collisions. The

centrality for Monte Carlo events was defined in accordance with the top cross section calculated using the transverse energy deposited in the TCal or PCal pseudorapidity region, as is done for the data. When using TCal  $E_t$  as a measure of centrality both event generators underpredict the peak value of the pseudorapidity density (Fig. 10 (a)). FRITIOF also overpredicts the position of the peak ( $\approx 2.2$  in comparison to the experimental value of 1.76). Similar trends were seen for FRITIOF results on pseudorapidity distributions of transverse energy [4]. In Fig. 10 (b) we compare the event generator predictions with the data using PCal  $E_t$  as a measure of centrality. Whereas the difference between FRITIOF results and the data remains almost the same as in Fig. 10 (a), the agreement between RQMD and data is significantly better. The origin of the different behavior is in the difference in the correlations between  $N_{ch}$  with TCal  $E_t$  and PCal  $E_t$  for the data and the event generators. The FRITIOF  $N_{ch} - \text{TCal } E_t$  and  $N_{ch} - \text{PCal } E_t$  correlations are close to the observed ones, and the results of comparison of pseudorapidity distributions is insensitive to the choice of TCal or PCal  $E_t$  as a measure of centrality. On the other hand RQMD exhibits a very tight  $N_{ch} - \text{PCal } E_t$  correlation, while the  $N_{ch} - \text{TCal } E_t$  correlation is rather loose. This results in lower mean  $N_{ch}$  for the events with highest TCal  $E_t$  in comparison with the mean value of  $N_{ch}$  for events with highest PCal  $E_t$ . Thus, for the same value of top cross section, the charged particle pseudorapidity densities for RQMD are quite different for the two cases.

### 4.3 Comparison with $dE_t/d\eta$ and evaluation of $E_t$ per charged particle

Below we combine multiplicity data with our earlier measurements [4] of  $dE_t/d\eta$  in Au+Au collisions at a similar, but not identical, energy. Due to the strong correlation between impact parameter and transverse energy produced in the central region (in our case PCal  $E_t$ ) it was found useful [4] to introduce the value  $E_t^0$ , the  $E_t$  for an average collision with impact parameter  $b < 0.5$  fm ( $\sigma_{top}(E_t^0)/\sigma_{geom} = 0.22\%$ ), and use the ratio  $E_t/E_t^0$  as a measure of centrality. For our case this yields  $E_t^0 \approx 318$  GeV. In Fig. 11(a) we present the charged particle pseudorapidity distributions for different PCal  $E_t$  regions centered approximately at  $E_t/E_t^0 = 0.2, 0.4, 0.6, 0.8,$  and  $1.0$ . The smooth curves represent Gaussian fits to the data. The peak position ( $\eta_{peak}$ ) and the width ( $\sigma_{eta}$ ) of Gaussian fits are presented in Fig. 11(b). The open circles in Fig. 11(b) show the dependence of parameters of Gaussian fit to  $dE_t/d\eta$  distributions from Ref. [4]. The peak position of  $dN_{ch}/d\eta$  is very close to that for  $dE_t/d\eta$ . It is smaller for lower centrality, presumably due to the relatively larger contribution of slow protons from the target. The width of the  $dN_{ch}/d\eta$  distribution decreases as centrality increases (similar to  $dN_{ch}/d\eta$  data for both the Au and Si beams), and is larger than the corresponding width of the  $dE_t/d\eta$  distribution.

We use the  $dE_t/d\eta$  distributions for the same centrality (value of  $E_t/E_t^0$ ) as shown in Fig. 11 to calculate  $E_t$  per charged particle as a function of pseudorapidity and centrality, and to compare them with RQMD and FRITIOF predictions (see Fig. 12). By  $E_t$  per charged particle we mean the ratio of

average value of total transverse energy to the average charged particle multiplicity  $E_t/N_{ch}$  (which is not the mean transverse energy of charged particles). Note that the value of transverse energy per charged particle is less sensitive than the absolute pseudorapidity spectra to uncertainties in defining the centrality cuts for experimental and Monte Carlo generated events. The pseudorapidity dependence of  $E_t$  per charged particle shown in Fig. 12(a) was calculated as a ratio of Gaussian fits to  $dE_t/d\eta$  [4] and  $dN_{ch}/d\eta$  distributions. The observed large value of  $E_t$  per charged particle about 0.75 GeV (for central collisions and in the central pseudorapidity region) is rather remarkable. If we take into account that the  $dE_t/d\eta$  spectra were measured at slightly higher energy (11.4 GeV/nucleon compared to 10.8 GeV/nucleon for current data) and re-scale  $E_t$  per charged particle with the available energy [1], which differs for both cases by approximately 4%, we get the value of 0.72 GeV. This value is significantly higher than that in p+Pb (about 0.45 GeV [13]), Si+Al and Si+Pb collisions (0.55–0.59 GeV and 0.52–0.54 GeV, respectively [2,4]) at an even higher beam energy of  $\approx 14.6$  GeV/nucleon. Note that we compare the  $E_t$  per charged particle for the central events triggered on  $E_t$ . The pseudorapidity distributions in References [2] and [10] were studied as a function of total charged multiplicity and cannot be used directly; but using the correlation between multiplicity and PCal  $E_t$  it is possible to estimate the peak value of the distribution for collisions with the highest PCal  $E_t$ . For example, for Si+Pb collisions this estimate gives a value of approximately 115–120 particles per unit of pseudorapidity for central Si+Pb collisions. Combining this value with the peak value of  $dE_T/d\eta \approx 62$  GeV observed in [4] one finds the value of  $E_t$  per charged particle cited above.

The comparison of model calculations with the data shows that the RQMD event generator describes the pseudorapidity and nontrivial centrality dependence of  $E_t$  per charged particle rather well, although the generator predicts the peak position to be at a slightly higher value of pseudorapidity. It cannot be excluded that this apparent disagreement is in part due to the representation of  $dN_{ch}/d\eta$  and  $dE_t/d\eta$  as Gaussian functions and to the fact that the two data sets were taken at slightly different beam energies. FRITIOF does not reproduce the pseudorapidity dependence and, in disagreement with the data, shows no dependence on centrality.

The possible origin of rather high value of  $E_t$  per charged particle was studied using the RQMD event generator, since it exhibits a dependence on centrality and pseudorapidity which is quite similar to the data. For this purpose Si+Pb at 14.6 GeV/c and Au+Au at 11.4 GeV/c collisions were studied. It was found that centrality dependence is almost totally due to changes in transverse energy deposited by nucleons. For less central events (and the collisions of nuclei of very different sizes, such as Si and Pb) the relative contributions of target spectators is rather large, which causes a decrease in  $E_t$  per charged particle. The second reason for the difference in  $E_t$  per charged particle between central collisions of light and heavy projectiles is a difference in the ratio of charged to all final state particles (caused by different relative numbers of protons and neutrons). It was observed in this model, that the transverse energy of produced particles (pions, kaons) do not exhibit any strong dependence on incident energy (within the energy range considered), size of the target or projectile, and centrality of the collision.

## 5 Conclusion

We have presented an analysis of charged particle multiplicity distributions in collisions of Au projectiles with Au, U, Cu, and Al targets with different centralities. The results are corrected for beam movement, upstream interactions,  $\delta$ -ray production, and  $\gamma$ -conversions. In studying the correlation between charged multiplicity and energy deposited in the calorimeters, we observe little or no change in the fluctuations of charged multiplicity as a function of centrality and no large scale fluctuations between charged multiplicity and transverse energy deposited in the same pseudorapidity region. The maximum value of the charged particle pseudorapidity density for very central Au+Au collisions is close to 270 and about 5% larger for the U target. The transverse energy per charged particle grows with increasing centrality. For central Au+Au collisions it is close to 0.72 GeV, significantly higher than in p+Au or Si+Pb collisions.

The FRITIOF event generator underpredicts the number of produced particles in the central region. The peak of the FRITIOF pseudorapidity distribution occurs at a much larger value of pseudorapidity than in the data. RQMD also underpredicts the charged particle density if one selects central events using transverse energy in the target region. If transverse energy in the central pseudorapidity region is chosen as a measure of the centrality, the description is better. The reason for this lies in the looser correlation between multiplicity and transverse energy in the target fragmentation region in the events generated by RQMD, in comparison with the data. The RQMD description of the centrality dependence of  $E_t$  per charged particle (calculated

in the region  $1.5 < \eta < 2.0$ ) is rather good; considering the pseudorapidity dependence of  $E_t$  per charged particle calculated for central collisions RQMD predicts the peak position of the distribution at slightly higher pseudorapidity value than data does. It is likely that the degree of re-scattering is even more important in the multiparticle production in heavy nucleus collision than it is implemented in the event generators; thus the production of thermalized hadron matter is more probable in such collisions.

## **Acknowledgments**

This research was supported, in part, by the U.S. DOE, the NSF, and Natural Sciences and Engineering Research Council of Canada.

## Appendix A: Correction for $\gamma$ -conversion

Let us denote by  $n$  the mean charged particle multiplicity in a particular pad;  $n$  is the quantity of interest. The  $\gamma$ -conversions to  $e^+e^-$ -pairs result in additional hits in the pad characterized by the mean multiplicity of uncorrelated (from different pairs) particles  $n_{\gamma 1}$  and mean number of pairs  $n_{\gamma 2}$ , when both the  $e^+$  and  $e^-$  from the pair occupy the same pad. In terms of these quantities the probability of a pad not being occupied (the input for the current analysis) is:

$$p_0 = 1 - e^{-n-n_{\gamma 1}-n_{\gamma 2}}. \quad (9)$$

The corresponding (to Poisson statistics) effective mean multiplicity equals:

$$\tilde{n} = -\ln(1 - p_0) = n + n_{\gamma 1} + n_{\gamma 2}. \quad (10)$$

To obtain the value  $n$  one should subtract from  $\tilde{n}$  not the true mean number of  $e^+$  and  $e^-$  from  $\gamma$ -conversions ( $n_e = n_{\gamma 1} + 2n_{\gamma 2}$ ), but the number of “apparent” particles, considering the pairs occupying the same pad as one particle ( $n_{\gamma 1} + n_{\gamma 2}$ ).

The distortion to Poisson statistics for multiple hits in the same pad due to  $\gamma$ -conversions can be evaluated from the probabilities of single and double hits:

$$p_1 = (n + n_{\gamma 1})e^{-n-n_{\gamma 1}}(1 - e^{-n_{\gamma 2}}), \quad (11)$$

$$p_2 = (n + n_{\gamma 1})^2 e^{-n-n_{\gamma 1}}(1 - e^{-n_{\gamma 2}})/2 + n_{\gamma 2}e^{-n_{\gamma 2}}(1 - e^{-n-n_{\gamma 1}}) \quad (12)$$



## Appendix B: Reconstruction of distribution from multilevel triggered data

Below we discuss a technique which permits the construction of unbiased experimental distributions from multilevel triggered data for the case where the variable of interest is weakly correlated with the variable on which the data are triggered. We make use of the expression which gives the distribution  $dw/dx$  in a quantity  $x$ , as an integral over the distribution  $dw/dy$  in another quantity  $y$ , on which the trigger decision is based:

$$\frac{dw}{dx} = \int \frac{dw}{dy}(y) \frac{dP}{dx}(x; y) dy, \quad (13)$$

where  $dP/dx(x; y)$  is the distribution in  $x$  for events at a fixed value of  $y$ . It is important to recognize that, whereas  $dw/dy$  is the distribution of the triggered quantity which is strongly influenced by downscaling (i.e. only a known fraction of the events above the trigger threshold are recorded), the function  $dP/dx(x; y)$  expresses the natural correlation between the two quantities and is independent of the trigger. If downscaling is introduced in the trigger, the distribution in  $y$  of the events which are written to tape is given by:

$$\frac{d\tilde{w}}{dy} = W(y) \frac{dw}{dy}, \quad (14)$$

where  $W(y)$  is the probability for the event with certain value of  $y$  to be written onto the tape and is constant within each trigger level region. We combine Eqs. (13)-(14) to obtain

$$\frac{dw}{dx} = \int \frac{1}{W(y)} \frac{d\tilde{w}}{dy}(y) \frac{dP}{dx}(x; y) dy, \quad (15)$$

which can be used directly for the calculation of distributions of quantities from multilevel triggered data. Eq. (15) has a very simple interpretation: in the calculation of distributions of some quantity  $x$  each event should be weighted with the inverse probability of the event being triggered. In other words, to calculate the natural distribution of events in  $x$ , we evaluate

$$\frac{\Delta N}{\Delta x} = \sum_{\text{events in } \Delta x} \frac{1}{W(y)}, \quad (16)$$

where the sum is taken over all triggered events written on tape with value of  $x$  within the region  $\Delta x$ .

## References

1. For a review of both CERN and AGS data, see J. Stachel and G. R. Young, *Annu. Rev. Nucl. Part Sci.* **42**, 237 (1992), and references quoted there.
2. E814 Collaboration, J. Barrette *et al.*, *Phys. Rev.* **C46**, 312 (1992).
3. E814 Collaboration, J. Barrette *et al.*, *Phys. Rev. Lett.* **64**, 1219 (1990).
4. E814/E877 Collaboration, J. Barrette *et al.*, *Phys. Rev. Lett.* **70**, 2996 (1993)
5. The details of PCal construction and calibration are given in J. Simon-Gillo *et al.*, *Nucl. Instrum. Methods* **A 309**, 427 (1991); D. Fox *et al.*, *Nucl. Instrum. Methods* **A 317**, 474 (1992);
6. E814 Collaboration, J. Barrette *et al.*, *Phys. Rev.* **C45**, 819 (1994).
7. E814 Collaboration, J. Barrette *et al.*, *Phys. Rev.* **C49**, 1669 (1994).
8. S. Hancock *et al.*, *Phys. Rev.* **A48**, 615 (1983); S. Hancock *et al.*, *Nucl. Instrum. Methods* **B1**, 16 (1984).
9. HELIOS Collaboration, T. Åkesson *et al.*, *Nucl. Phys.* **B333**, 48 (1990).
10. K. Jayananda, PhD Thesis, University of Pittsburgh, 1991
11. B. Andersson, G. Gustafson, and B. Nilsson-Almqvist, *Nucl. Phys.* **B281**, 289 (1987); the parameters for the AGS energies were taken from: J. Costales, E802 Internal report No. E-802-MEM-8, 1988 (unpublished).
12. H. Sorge, H. Stöcker, and W. Greiner, *Ann. Phys. (N.Y.)* **192**, 266 (1989).

13. E814 Collaboration, M. Rosati, Nucl. Phys., **A566**, 597c (1994); J. Barrette *et al.*, “Transverse energy and charged multiplicity in p-nucleus collisions at 14.6 GeV/nucleon”, E814/E877 preprint, 1994.

## Figure Captions

1. Experimental setup of E877 at BNL. For this analysis, we use data from the Multiplicity Detector, Target, and Participant calorimeters (see insert).
2. E877 Multiplicity Detector, consisting of two identical 300  $\mu\text{m}$  thick silicon disks, segmented into 512 pads. The combined pseudorapidity coverage is  $0.87 < \eta < 2.46$ .
3. Fits of the pulse height distributions by modified Landau distributions. Contribution from 1, 2, and 3 m.i.p. are shown. The dashed line indicates the Gaussian fit to the electronic noise.
4. Distribution of the horizontal (solid histogram) and vertical (dashed histogram) coordinates of the hit centroid as a function of the beam position measured in the Beam Vertex Detector. Straight lines represent linear fits to the distributions.
5. The dependence of mean number of hits in the Multiplicity Detector as a function of TCal  $E_t$  is shown for 1% (solid histogram) and 2% (dashed histogram) Au targets. The extrapolations to  $E_t = 0$  gives an estimate of the numbers of  $\delta$ -electrons.
6. Charged particle pseudorapidity distributions used as corrections for Au+Au collisions (1% target). (1) Distribution due to  $\gamma$ -conversions for TCal  $E_t$  region 22–28 GeV, (2) distribution of  $\delta$ -rays produced in

the target and in the absorbers, and (3) Distribution of  $\delta$ -rays from upstream material.

7. Transverse energy in TCal, PCal, and downstream energy deposited in UCal plotted *versus* the raw number of hits in the Multiplicity Detector. The crosses indicate the width ( $\sigma$ ) of the distributions in each variable.
8. (Top panel): Differential cross sections in TCal  $E_t$  for collisions of a Au projectile with U, Au, Cu, and Al targets. For clarity Au+Au, Au+Cu, and Au+Al cross sections are multiplied by factors of 0.1, 0.01, and 0.001 respectively. (Bottom panel): The cross section integrated above  $E_t$  (see Eq. 8 and text thereafter), normalized to the geometrical cross section.
9. Charged particle pseudorapidity distributions for different centralities (TCal  $E_t$  regions). For the most central region we show also the Gaussian fit to the distribution. (a) Au+Au collisions; (b) Au+U collisions; (c) Au+Cu and Au+Al collisions.
10. (1) Experimental charged particle pseudorapidity distribution for Au+Au collisions, compared with RQMD (2) and FRITIOF (3) predictions for the equivalent centrality; (a) TCal  $E_t$  energy region 22–28 GeV ; (b) PCal  $E_t$  energy region 310–330 GeV.
11. (a): Charged particle pseudorapidity distributions in Au+Au collisions for the different centralities (PCal  $E_t$  regions). The curves are Gaussian fits to the data. (b): Peak position and the width of the Gaussian fit

to  $dN_{ch}/d\eta$  as a function of centrality ( $E_t/E_t^0$ , for details, see text) in comparison with parameters of the analogous fits to  $dE_t/d\eta$  [4], shown as open circles.

12. Transverse energy per charged particle for Au+Au collisions, compared with predictions from RQMD and FRITIOF. The data are derived from Gaussian fits to  $dE_t/d\eta$  taken at 11.4 GeV/nucleon and  $dN_{ch}/d\eta$  taken at 10.8 GeV/nucleon, as discussed in the text. (a) pseudorapidity dependence for central events (PCal  $E_t$  energy region 310–330 GeV); (b) PCal  $E_t$  dependence of  $E_t$  per charged particle in the region  $1.5 < \eta < 2.0$ .

This figure "fig1-1.png" is available in "png" format from:

<http://arxiv.org/ps/nucl-ex/9412003v2>



This figure "fig1-2.png" is available in "png" format from:

<http://arxiv.org/ps/nucl-ex/9412003v2>

This figure "fig1-3.png" is available in "png" format from:

<http://arxiv.org/ps/nucl-ex/9412003v2>

This figure "fig1-4.png" is available in "png" format from:

<http://arxiv.org/ps/nucl-ex/9412003v2>

This figure "fig1-5.png" is available in "png" format from:

<http://arxiv.org/ps/nucl-ex/9412003v2>

This figure "fig1-6.png" is available in "png" format from:

<http://arxiv.org/ps/nucl-ex/9412003v2>

This figure "fig1-7.png" is available in "png" format from:

<http://arxiv.org/ps/nucl-ex/9412003v2>

This figure "fig1-8.png" is available in "png" format from:

<http://arxiv.org/ps/nucl-ex/9412003v2>

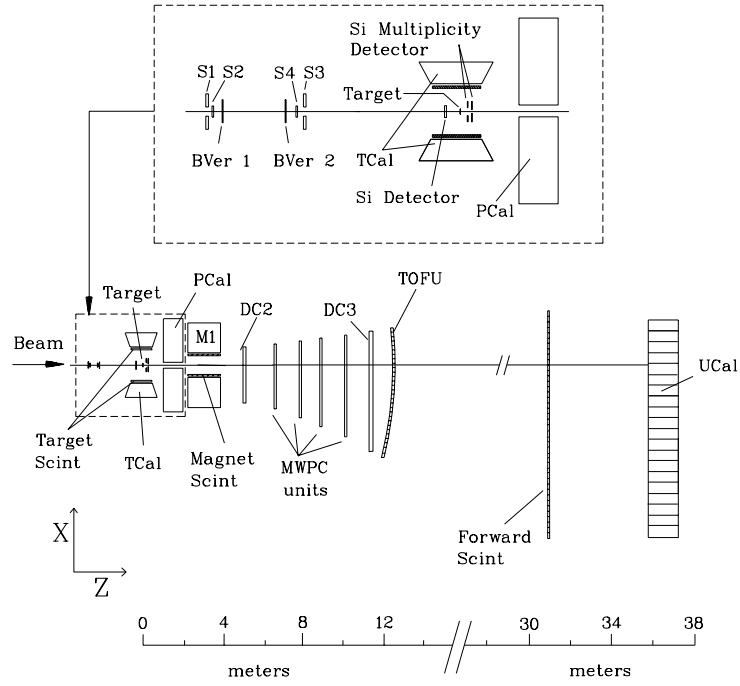


Figure 1:

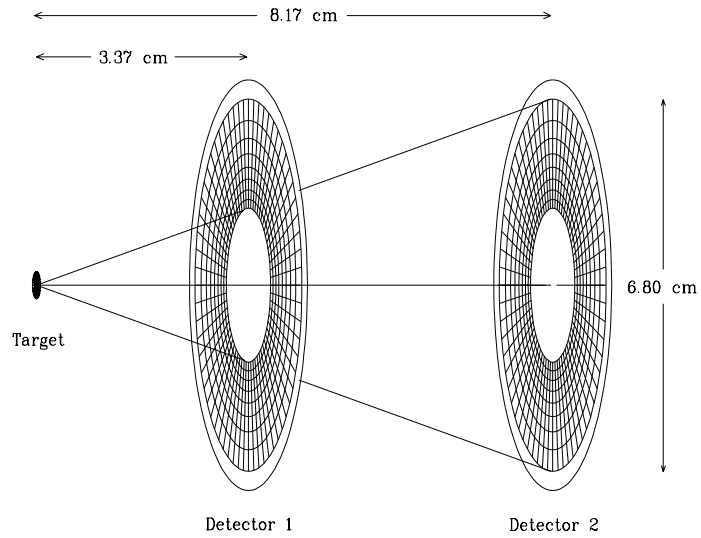


Figure 2:



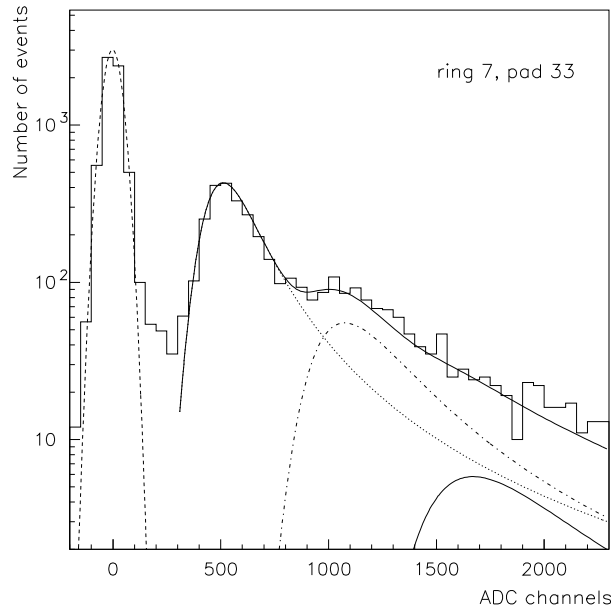


Figure 3:

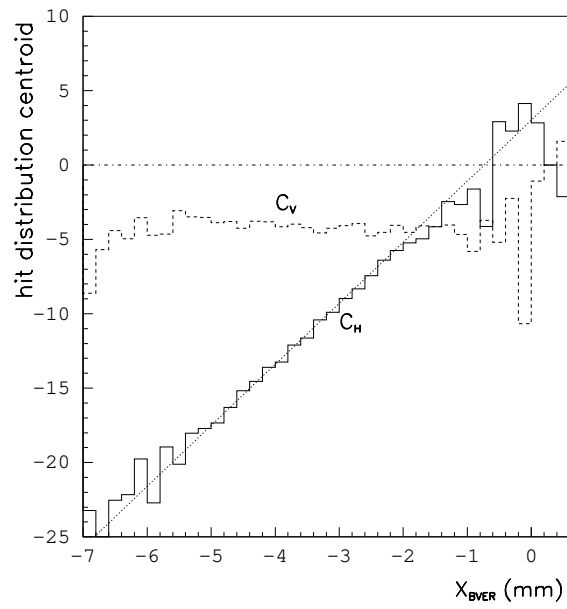


Figure 4:

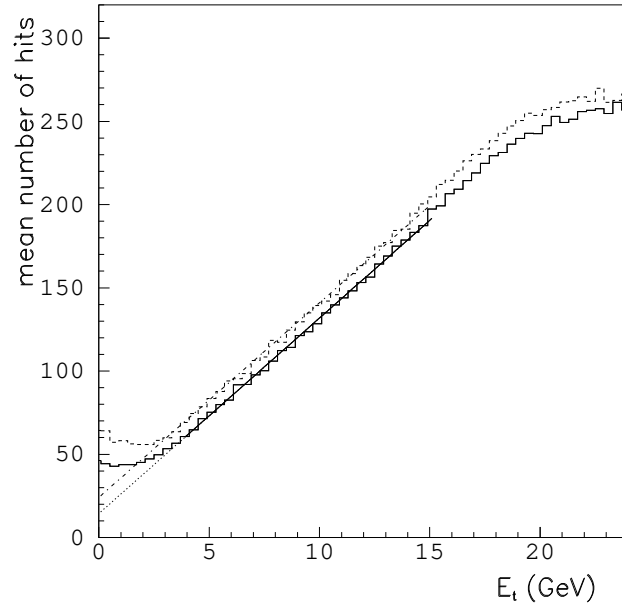


Figure 5:

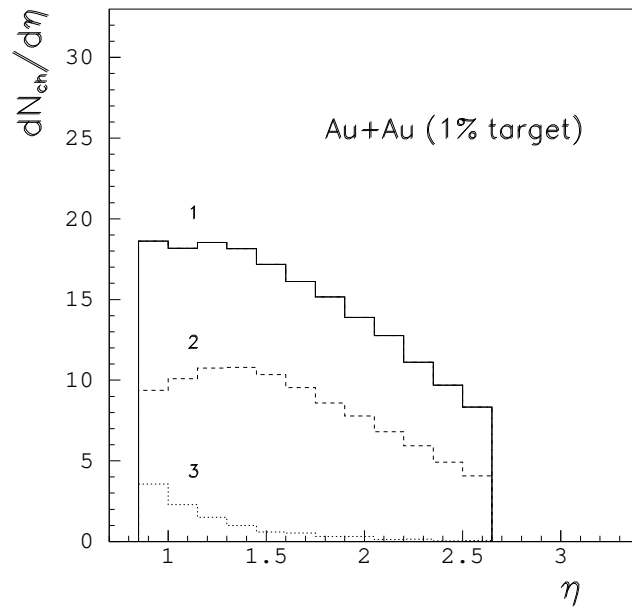


Figure 6:

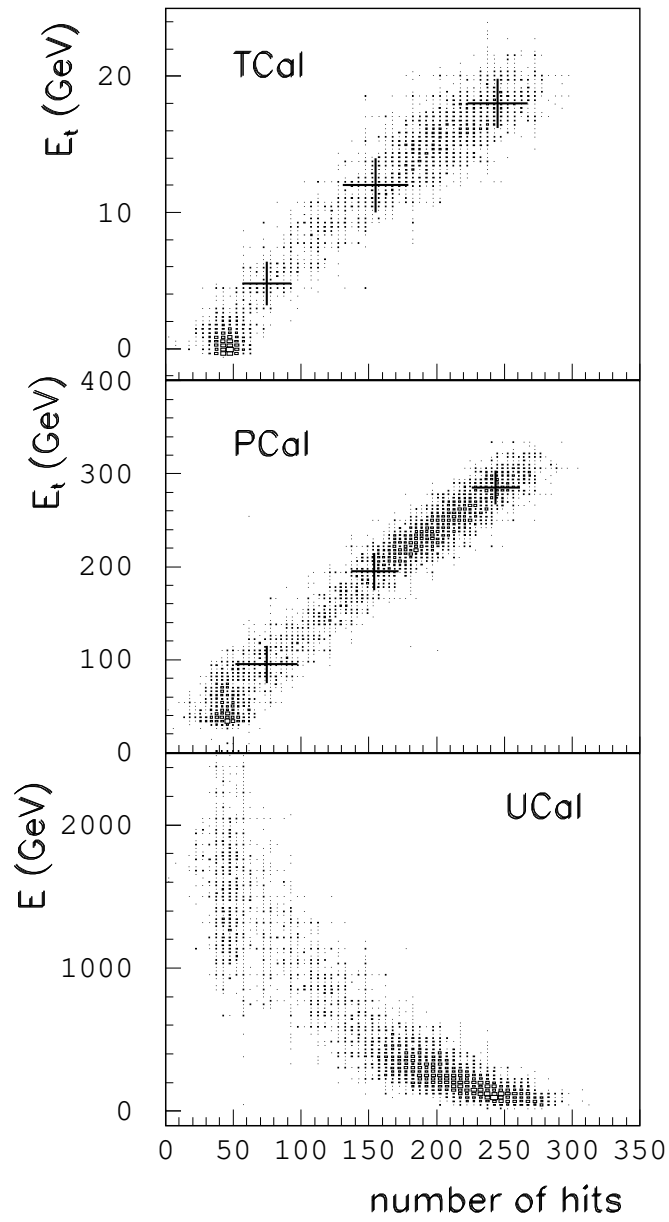


Figure 7:

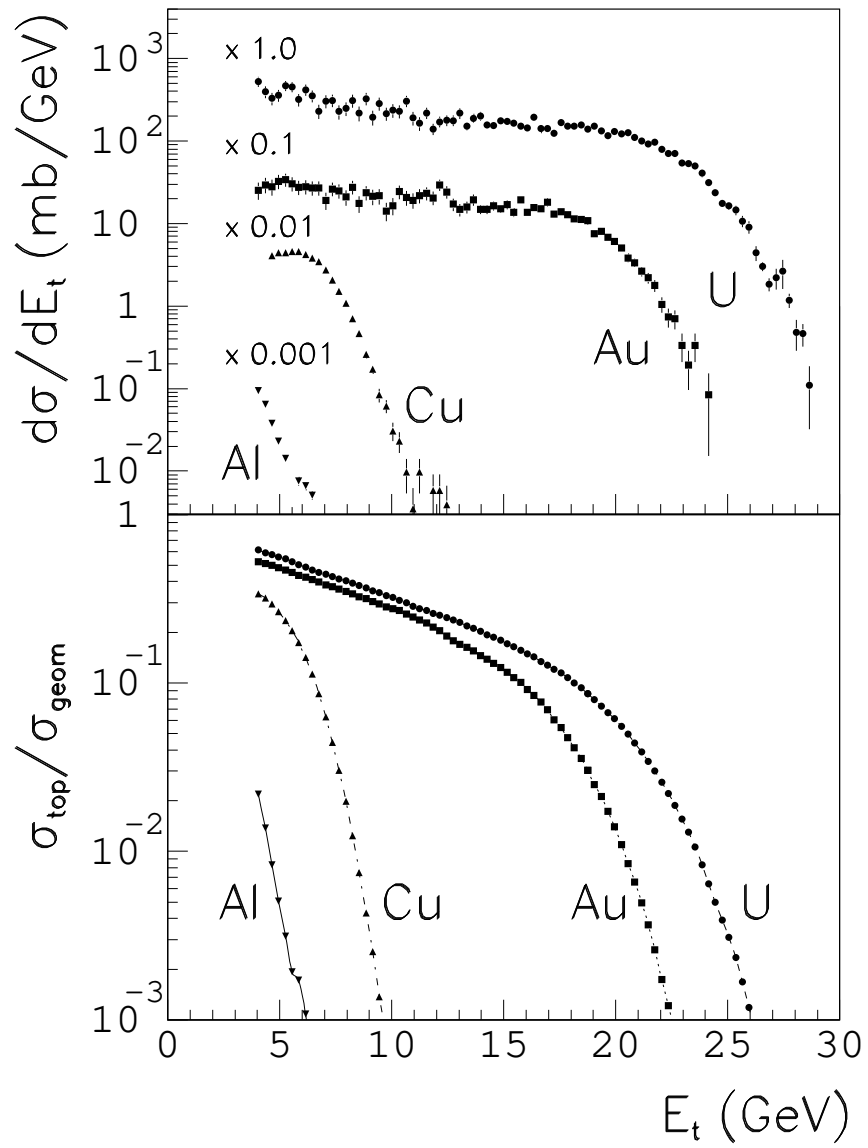


Figure 8:

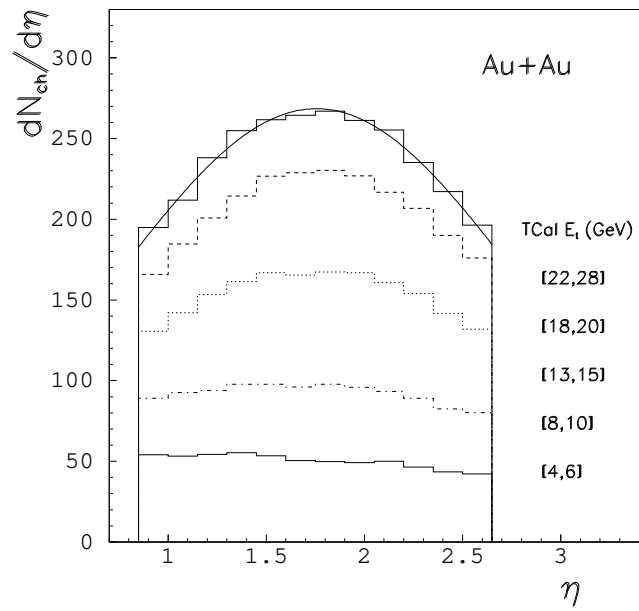


Figure 9 (a):

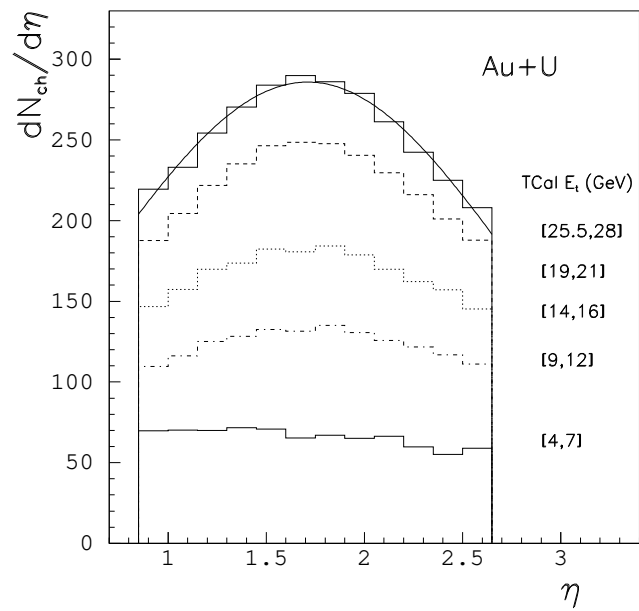


Figure 9 (b):

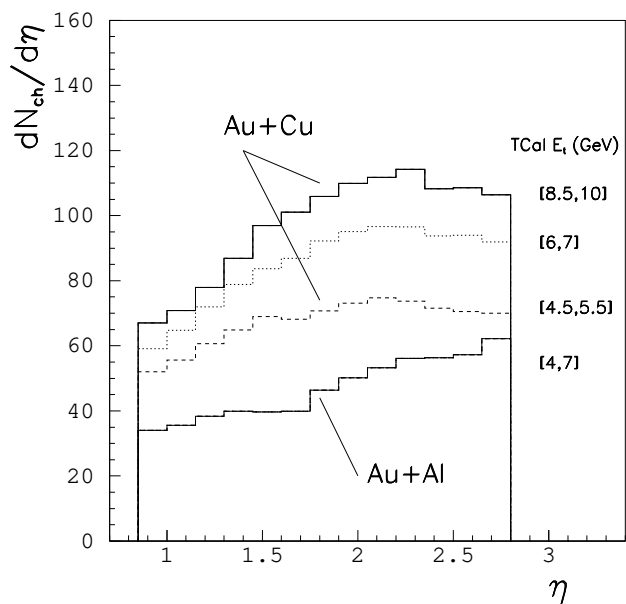
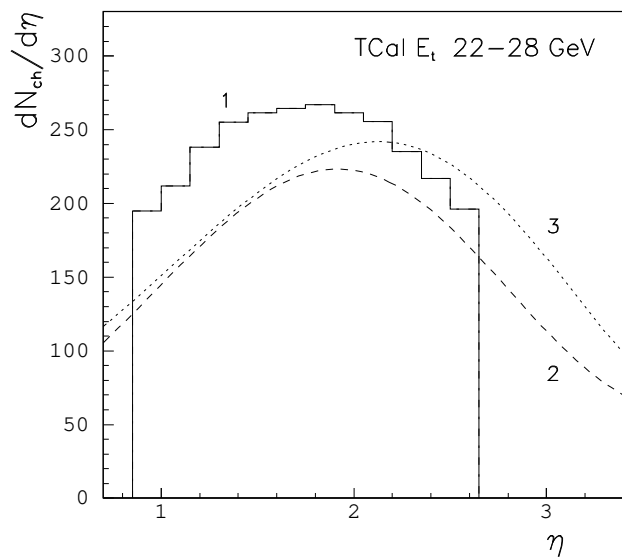
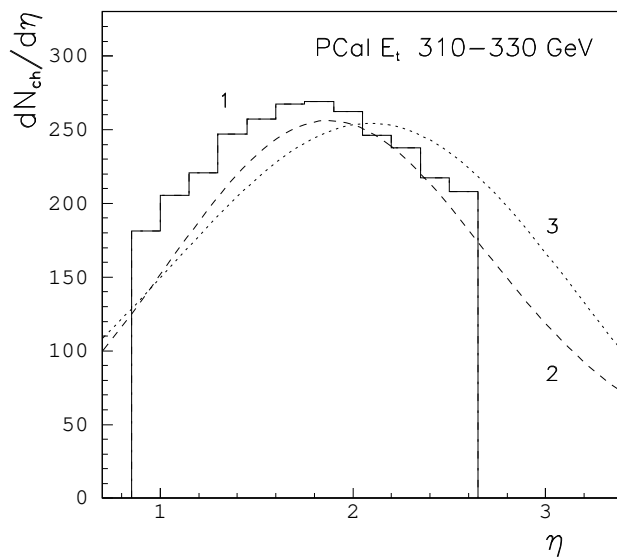


Figure 9 (c):



(a)



(b)

Figure 10:

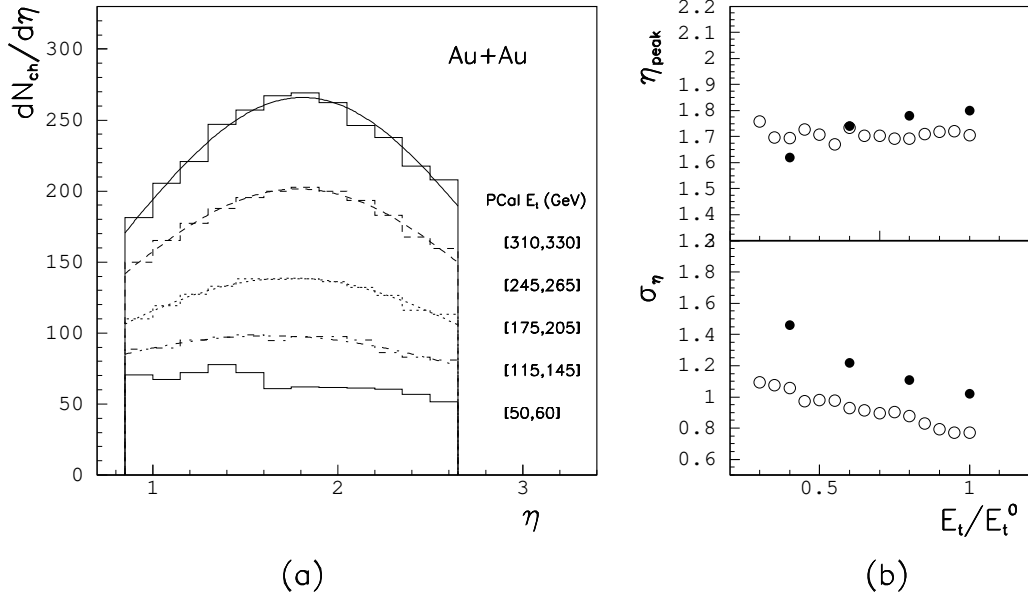


Figure 11:

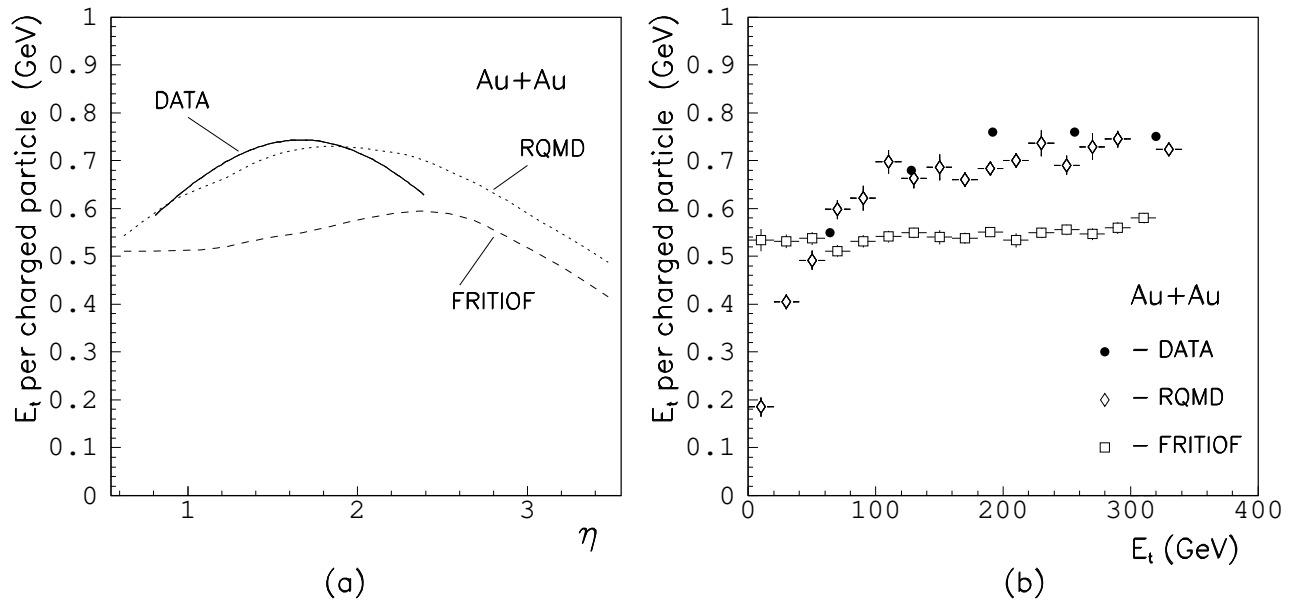


Figure 12: